IEEE Access
Multidisciplinary | Rapid Review | Open Access Journal

Received November 16, 2019, accepted November 27, 2019, date of publication December 5, 2019,
date of current version December 23, 2019.

Digital Object Identifier 10.1109/ACCESS.2019.2957890

Enhanced Performance of a Stand-Alone Gas-Engine Generator Using Virtual Synchronous Generator and Energy Storage System

HTAR SU HLAING[1], JIA LIU[1], (Member, IEEE), YUSHI MIURA[2], (Member, IEEE), HASSAN BEVRANI[3], (Senior Member, IEEE), AND TOSHIFUMI ISE[4], (Member, IEEE)

[1]Electrical, Electronics, and Information Engineering Department, Osaka University, Suita 565-0871, Japan
[2]Electrical, Electronics, and Information Engineering Department, Nagaoka University of Technology, Niigata 940-2188, Japan
[3]Department of Electrical and Computer Engineering, Smart/Micro Grids Research Center, University of Kurdistan, Sanandaj, Iran
[4]NARA-GAKUEN Incorporated Educational Institution, Nara 636-8503, Japan

Corresponding author: Jia Liu (liu@eei.eng.osaka-u.ac.jp)

ABSTRACT Gas engine generators have been recognized as a set of beneficial generating units for producing electric power owing to their high efficiency, low emissions and appropriate fuel price. However, the major drawback of gas engine generators is the weak transient performance during sudden load change. The reason is that the engine's mechanical system cannot quickly respond to the demanded torque. Therefore, a change in load causes a large engine speed deviation, especially in stand-alone mode. If the engine speed deviation exceeds the allowable limits, the system operation will be shut down. To fix this drawback, this paper introduces the virtual synchronous generator control method combined with an additional energy storage system to the stand-alone gas engine generator. In this paper, the applied virtual synchronous generator control scheme is presented. Compared to the constant-voltage constant-frequency control method, the benefit of virtual synchronous generator control method for the gas engine generator is evaluated by simulation study in PSCAD software. The energy-variables-based feedback control structure is adopted for the control of energy storage system. The required capacity of energy storage system is estimated. To verify the effectiveness of proposed control structure, simulation is conducted under load connection and load removal cases. Finally, an experimental study is carried out for the same configuration of simulation model using a real gas-engine generator set up.

INDEX TERMS Gas engine generator, virtual synchronous generator, energy storage system, transient response.

I. INTRODUCTION

Gas engines are widely used in the field of emergency power and combined heat and power applications. They can also serve as main power sources in places where utility power is not available. Moreover, compared to diesel engines, gas engines are more environment-friendly as they release low exhaust emissions. Despite the effectiveness of gas engines, they cannot fully provide their advantages to the system. The reason is the engine's delayed response to sudden load power change. The gas engine has a time constant of a few second to reach the demanded torque due to fuel injection function. Consequently, the speed deviation is large during load transitions. If the speed variation is larger than the permitted limits, the operation will be shut down. Therefore, for the current users of gas engines, the load step capability is restricted in order to maintain the engine speed variation within the allowable limits. For this reason, the transient behavior of gas engine is a major challenge in using gas engines. The general transient response requirements of gas engines are presented in [1]. The step load responses of two types of gas engines and one diesel engine are also compared in [1]. The results show that the gas engine has longer recovery time and larger frequency excursion than the diesel engine. In [2], the start-up time reduction of gas engine is analyzed in order to increase the transient response of gas engine. As an option of providing the demanded power without delay, the use of energy storage system (ESS) in combination with engine is

The associate editor coordinating the review of this manuscript and approving it for publication was Amjad Anvari-Moghaddam.

suggested. This option is a solution to the transient issues that deal with the slow response of engine's thermal and mechanical system by the help of electrical system.

The frequency regulation of two parallel-connected gas engine generator sets with the addition of ESS is presented in [3].The use of ESS in combination with diesel engine is also found in [4] and [5]. In [4], the dynamic behavior of stand-alone diesel engine generator set with ESS is studied. However, the study is done only under load connection case. The dynamic characteristic of the system for load removal case is not described. As for stand-alone system, the transient characteristics of load removal case are necessary to be investigated. Also in [5], the dynamic behavior of variable-speed diesel engine generator set is analyzed, and the encountered problems during a sudden load increase are solved by using an ESS. In [6], the ESS is used for the dynamic frequency control support of isolated wind and solar power generation. In [4]–[6], the advantage of using an ESS to improve the dynamic performance of an isolated power system is well established. However, the inverter control algorithm is based on conventional constant-voltage constant-frequency (CVCF) control.

Recently, the concept of virtual synchronous generator (VSG) control method which can control inverter to behave like a synchronous generator (SG) has been developed. In this control method, the swing equation of a typical SG is realized in the inverter control scheme, and the energy storage connected to the inverter imitates the kinetic energy of rotating mass. Usually, the energy storage is a dc link capacitor. In some cases where the large amount of energy is required, a battery or a supercapacitor can be added to the dc link capacitor. In this case, the VSG control method exhibits virtual inertia and supports a smooth power transition. Moreover, similar to an SG, the VSG control can be automatically synchronized with the grid and provide inertia support for the utility [7]–[9]. In most previous research works, the VSG method is employed either without considering the feature of energy resources [10]–[16], or only focused on grid-connected systems [17]–[23]. Only some research works are focused on using the VSG method for stand-alone system considering the feature of the energy resources [24]–[26]. In [24], the VSG control is proposed for the control of grid side converter for a full converter wind turbine (FCWT). The proposed VSG control allows the system to operate under both grid-connected and stand-alone conditions. In [25], the problems of matching photovoltaic (PV) output and load as well as dc voltage collapse are solved by the VSG control in a stand-alone PV system. In [26], the VSG control is applied for the load side inverter control of the stand-alone gas-engine generator system.

Following the above mentioned advantages of ESS and VSG control, in this paper, the VSG control with an additional ESS is proposed for the stand-alone gas engine generator system. The proposed gas-engine generator system is shown in Fig. 1. The system consists of a gas engine, a Permanent Magnet Synchronous Generator (PMSG), a simple full-wave

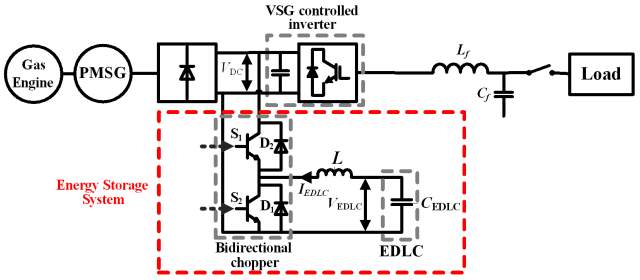

FIGURE 1. Configuration of proposed gas engine generator system.

diode rectifier, a dc link capacitor, an inverter and the load. The ESS is connected to the dc link via a bidirectional chopper. In this study, the capacity of ESS is calculated based on the demanded load power to deliver adequate energy during load transients. An energy-variables-based feedback control structure is adopted for the bidirectional chopper control. The control scheme of VSG is introduced and the benefit of VSG control for the stand-alone gas engine system is discussed. The transient performance of the proposed system is analyzed under sudden load change conditions by both simulation and experimental studies.

The rest of the paper is organized as follows. Section II describes the control scheme of VSG used in this study. In section III, the benefit of VSG control method for the proposed system is evaluated by the comparison with a CVCF control method. The control structure for energy storage is proposed in section IV. Calculation of energy storage capacity is presented in section V. The simulation results are discussed in section VI and the experimental results are presented in VII. Finally in section VIII, the paper is concluded.

II. VSG CONTROL SCHEME

The VSG control scheme proposed in [26] is shown in Fig. 2. In this figure, the "Swing Equation Function" block emulates the function of swing equation of an SG as expressed in (1).

$$P_{in} - p_{out} = J\omega_m \frac{d\omega_m}{dt} - D\Delta\omega_m \tag{1}$$

where P_{in} and P_{out} are input power and output power, respectively; J is the inertia moment, D is the damping factor, ω_m is the virtual angular velocity of virtual rotor, $\Delta\omega_m$ is the slip between virtual angular frequency and the frequency of inverter output voltage ($\omega_m - \omega_{V-inv}$), which is used to mimic the dynamics of damper windings during transients.

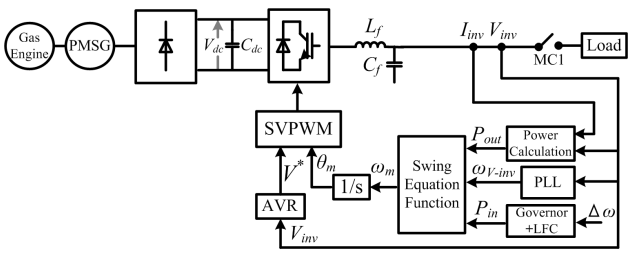

FIGURE 2. VSG control scheme.

Here, the phase-locked loop (PLL) is used for detecting ω_{V-inv}. As for stand-alone system, ω_m determines the frequency of the network and ω_{V-inv} follows ω_m.

Instead of PLL, one may use other simpler detectors. However, in the stand-alone system application, there is no need to worry about the oscillatory issues of the PLL. Because the PLL oscillatory dynamic is mostly appeared when the PLL is used to synchronize the inverter with an external voltage source, which is not the presented case. The PLL dynamics can affect the damping property, if a large damping factor D is used, as it is discussed in [16], where $D = 156$ pu. However, for a small $D = 17$ pu used in this paper, the negative impact is negligible. On the other hand, the adopted value of D can still provide enough damping effect for stand-alone applications, as it is demonstrated in the authors previous works [12], [13], and [27].

The values of J and D are defined in the inverter control program as the inverter does not have a rotating mass. Then, the swing equation is solved in the control program and ω_m is obtained. To solve swing equation, the forth-order Runge-Kutta iterative algorithm is used to obtain the change of ω_m over a time step Δt. By integrating ω_m, the phase reference θ_m for the output voltage of the inverter is calculated. In the block "Power Calculation", the active power P_{out} is calculated from inverter output voltage and inverter output current using (2). The line-to-line RMS value of inverter output voltage V_{inv} is calculated by (3).

$$P_{out} = v_{inv\_a} i_{inv\_a} + v_{inv\_b} i_{inv\_b} + v_{inv\_c} i_{inv\_c} \quad (2)$$

$$V_{inv} = \sqrt{v_{inv\_a}^2 + v_{inv\_b}^2 + v_{inv\_c}^2} \quad (3)$$

Like a typical SG, the automatic voltage regulator (AVR) is used to regulate the actual inverter voltage V_{inv} to match the inverter base voltage $V_{\text{inv}}{}^*$. The output of AVR is the voltage magnitude reference V^* for inverter output voltage. The block diagram of AVR is shown in Fig. 3. A governor function can also be performed in VSG control scheme for the control of the load-power as shown in Fig. 4.

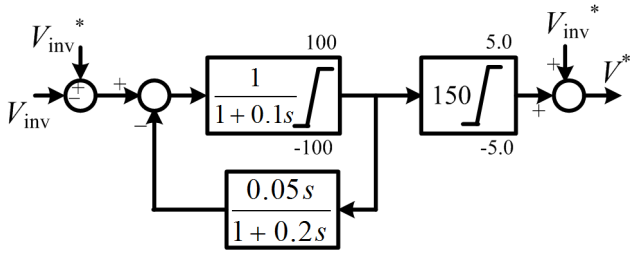

FIGURE 3. Block diagram of AVR.

In this study, a simple first-order lag represents the governor function and δ is the droop coefficient in percent. However, if the load variations occur, the frequency deviates from the base frequency due to the droop characteristic of governor. Therefore, the load-frequency control (LFC) is incorporated with the governor control in order to maintain the frequency at the inverter base frequency, f_{inv_0}, in case of load fluctuations.

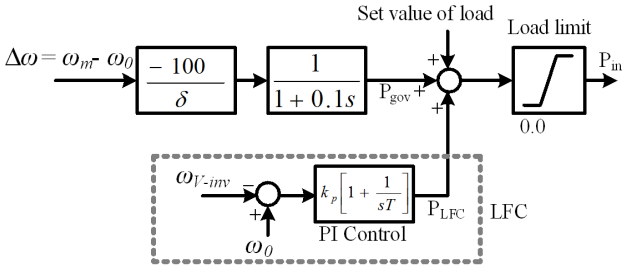

FIGURE 4. Governor and load-frequency control.

III. EVALUATING OF VSG CONTROL RESPONSE IN STAND-ALONE GAS ENGINE SYSTEM

In this section, the benefit of VSG control for stand-alone gas engine is evaluated by simulation study. The evaluation is done for the sudden load increase case. The results of system responses are compared to the results of the same system with the CVCF control method. The aim of this evaluation is to analyze the characteristics of VSG control and CVCF control for stand-alone system. Therefore, an external ESS is not added to the dc link capacitor. The system configurations with the respective control scheme are shown in Fig. 2 and Fig. 5. As the gas engine is operating in the stand-alone mode, the effect of VSG control is more obvious in the case of frequency dependent load compared to the case of frequency independent load. Therefore, in order to clarify the advantage of VSG over CVCF control, an induction motor is used for both the cases. The parameters of induction motor (as a frequency dependent load) are shown in Table 1.

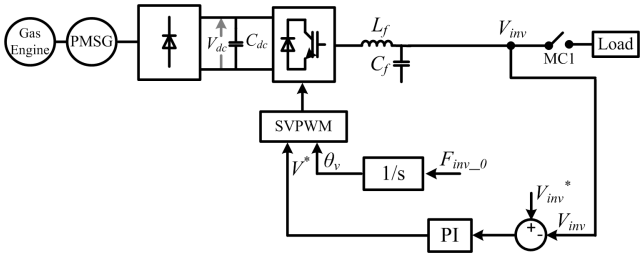

FIGURE 5. CVCF control scheme.

The simulations are performed for both the systems under the step loading condition. The simulation results for engine speed and generator output power following a sudden load-power increase are shown in Fig. 7.

In the simulation study, the gas engine model is simplified by combining the engine time delay and the settling time of speed controller. Therefore, a simple PI speed controller shown in Fig. 6 represents the engine model. The parameters of the speed controller, the PMSG and the VSG control scheme are listed in Tables 2 and 3, respectively. These parameters are set to be close to the test result of engine speed response when the engine operates without using the ESS. For the system with CVCF control, the parameters of proportional-integral (PI) controller are selected as $k_{\text{p}} = 0.008$ s and $T_{\text{i}} = 1$.

Before 20 s, the system is running with no load and the engine speed is maintained at its rated speed of 1710 min^{-1}.

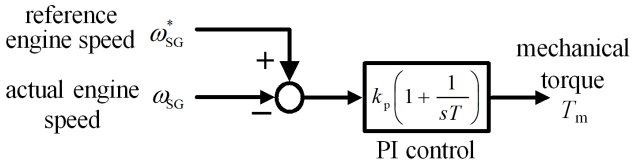

FIGURE 6. Simplified speed control block that represents gas engine.

TABLE 1. Parameters of induction motor load.

Rated power	9 kW	Angular speed	377 rad/s
Rated volatge	200 V	Per-unit inertia constant M	10 s
Rated current	26 A		

TABLE 2. Parameters of synchronous generator and speed control.

X_d	0.219 pu	X_q	0.219 pu
X_d'	0.027 pu	X_q'	0.027 pu
T_{do}'	6.55 s	T_{qo}'	0.85 s
X_d''	0.01 pu	X_q''	0.01 pu
T_{do}''	0.039 pu	T_{qo}''	0.071 pu
Base power	10 kW	Base voltage	210 V
Engine speed command ω_{SG}^*	1710 min^{-1}	Per-unit inertia constant	0.08 s
Speed control PI gain k_{pG}	0.035	Speed control PI time constant T_G	1.0 s

TABLE 3. Parameters of VSG control.

Base Power P_{base}	10 kW	Base voltage V	200 V
Base Frequency f_{inv_0}	60 Hz	Speed regulation factor δ	5 %
Per-unit inertia constant M	10 s	Inertia moment J	0.7036 kg.m^2
Damping Factor D	17 pu	Inverter switching frequency f	15 kHz
LFC PI gain	20	LFC PI time constant	0.5 s
Output voltage command V_{inv}*	200 V		

At 20 s, the load is connected to the system and the engine speed decreases suddenly in both cases as shown in Fig. 7 (a). In both cases, the speed recovers to its rated value after 2 s. However, the amount of speed dip under VSG control is nearly 80 min^{-1} smaller than the case with CVCF control. Moreover, there are some oscillations in the engine speed waveform of the case with CVCF control while there are no oscillations in the waveform of the case with VSG control. The simulation results of generator output power for both cases are shown in Fig. 7 (b). At the start of loading, there is a small overshoot and some oscillations in the waveform of the case with CVCF control. In case of VSG control, the power changes in a smooth way at the instant of loading. These simulation results show that the engine speed variations and generator output power changes can be properly damped by using the VSG control due to the effect of virtual inertia. Therefore, the proposed VSG control for the stand-alone

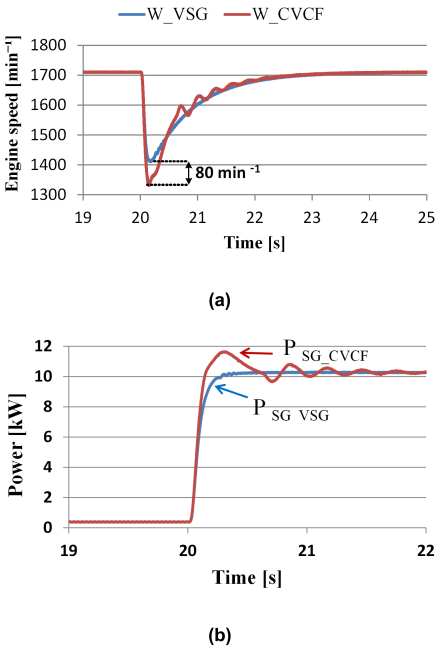

FIGURE 7. Simulation results of loading condition comparing VSG control and CVCF control. (a) Engine speed. (b) Generator output power for loading case.

operation of gas engine generator provides a significantly improved transient performance.

IV. ENERGY STORAGE SYSTEM CONTROL STRUCTURE

The ESS is connected to the dc link of the system. As mentioned, the purpose of this study is to improve the characteristics of the gas engine generator under transient conditions, and therefore it is necessary to supply energy in a short time. The Electric Double Layer Capacitor (EDLC) has the characteristics that it can send a large amount of energy in a short time. For this reason, the EDLC is used as an energy storage device in this study.

For both loading and load removal cases, the energy of EDLC should be recovered to the original amount level after the system has reached to its steady state. Therefore, an energy-variables-based feedback control strategy is proposed for controlling energy transfer between EDLC and dc link as shown in Fig. 8. In Fig. 8, the proposed control structure is composed of three control loops. In the energy recovery control loop, the actual EDLC energy W_{EDLC} is compared with the reference W_{EDLC}* and the error is sent to a proportional controller. The output of proportional controller is the recovery power of EDLC, P_{R_EDLC}, and is sent to the EDLC power control loop. In the EDLC power control loop, P_{EDLC}* is the reference EDLC power. The error of P_{EDLC} is

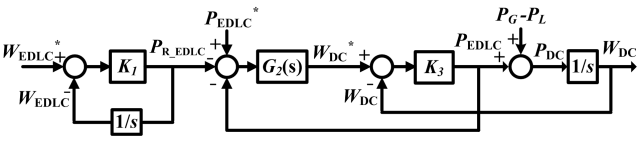

FIGURE 8. Feedback control structure for energy storage.

the input of a PI controller, and the output of PI controller is the reference value for the dc link energy control. In the dc link energy control loop, $W_{DC}{}^*$ is the reference dc link energy and W_{DC} is the actual dc link energy. The error of W_{DC} is sent to a proportional controller and the output of the controller is the EDLC power P_{EDLC}.

In this control structure, the design of time constants is a key point and thus in the following subsections, the settings of time constants are explained.

A. DC LINK ENERGY CONTROL

The control loop of dc link energy control can be illustrated as shown in Fig. 9. In this diagram, P_G is the generator output power, P_L is the load power, P_{DC} is the dc link power, K_3 is the gain and s is the Laplace operator.

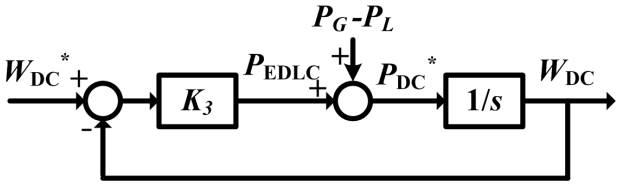

FIGURE 9. Dc link energy control block diagram.

When the generation-load mismatch (P_G - P_L) is considered as a disturbance and the closed-loop transfer function can be obtained as follows.

$$\left(W_{DC}^* - W_{DC}\right)\frac{K_3}{s} = W_{DC}$$
$$\Leftrightarrow \frac{K_3}{s}W_{DC}^* = W_{DC}\left(1+\frac{K_3}{s}\right) \quad (4)$$

From (4), the transfer function for dc link energy control is derived as in (5).

$$\frac{W_{DC}}{W_{DC}^*} = \frac{\frac{K_3}{s}}{1+\frac{K_3}{s}} = \frac{1}{1+\frac{1}{K_3}s} = \frac{1}{1+sT_3} \quad (5)$$

where the time constant is expressed as in (6).

$$T_3 = \frac{1}{K_3} \quad (6)$$

B. EDLC POWER CONTROL

The control loop diagram for EDLC power control is shown in Fig. 10.

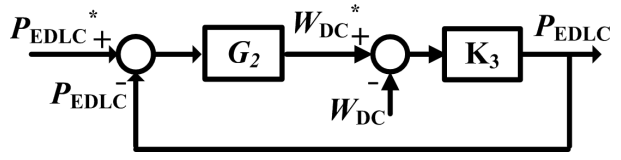

FIGURE 10. *EDLC* power control block diagram.

From Fig. 10, the transfer function of EDLC power control loop can be written as follows:

$$\left(W_{DC}^* - W_{DC}\right)K_3 = P_{EDLC} \quad (7)$$
$$\left(P_{EDLC}^* - P_{EDLC}\right)G_2(s) = W_{DC}^* \quad (8)$$

In steady state, $P_{EDLC}{}^*$ is zero. By substituting (8) into (7), the following relationship can be obtained

$$\left(-G_2(s)P_{EDLC} - W_{DC}\right)K_3 = P_{EDLC}$$
$$\Leftrightarrow -W_{DC}K_3 = P_{EDLC}\left(1+G_2(s)K_3\right) \quad (9)$$

and

$$P_{EDLC} = -\frac{K_3}{1+G_2(s)K_3}W_{DC} \quad (10)$$

When $G_2(s) = K_p(1+1/sT_2)$, where K_p is a proportional gain and T_2 is an integral time constant, (10) can be rewritten as (11).

$$P_{EDLC} = -\frac{sT_2K_3}{K_3K_p + s\left(1+K_3K_p\right)T_2}W_{DC} \quad (11)$$

If W_{DC} in (11) is considered as a unit step input, P_{EDLC} becomes

$$P_{EDLC} = -\frac{sT_2K_3}{K_3K_p + s\left(1+K_3K_p\right)T_2}\frac{1}{s}$$
$$= \frac{-\frac{K_3}{(1+K_3K_p)}}{s+\frac{K_3K_p}{(1+K_3K_p)T_2}} \quad (12)$$

Finally, using inverse Laplace transform, the unit step response of P_{EDLC} can be obtained as follows.

$$P_{EDLC} = -\frac{K_3}{\left(1+K_3K_p\right)}\exp\left\{-\frac{K_3K_p}{\left(1+K_3K_p\right)T_2}t\right\} \quad (13)$$

C. EDLC ENERGY RECOVERY CONTROL

The EDLC energy recovery control loop is shown in Fig. 11. The time constant T_1 of this control loop is derived as follows:

$$\left(W_{EDLC}^* - W_{EDLC}\right)\frac{K_1}{s} = W_{EDLC}$$
$$\Leftrightarrow \frac{K_1}{s}W_{EDLC}^* = W_{EDLC}\left(1+\frac{K_1}{s}\right) \quad (14)$$

where K_1 is the proportional gain.

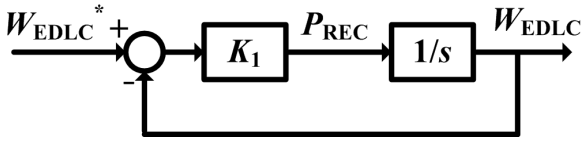

FIGURE 11. EDLC energy recovery control block diagram.

From (14), the transfer function for EDLC energy control is obtained as given in (15).

$$\frac{W_{EDLC}}{W_{EDLC}^*} = \frac{\frac{K_1}{s}}{1+\frac{K_1}{s}} = \frac{1}{1+\frac{1}{K_1}s} = \frac{1}{1+sT_1} \quad (15)$$

where the time constant is expressed as

$$T_1 = \frac{1}{K_1} \quad (16)$$

The time constant of each control loop is derived as explained above. Among the three control loops, the fastest

response is required for the dc link energy W_{DC} control loop. The slowest response is for the EDLC energy recovery control loop. Therefore, T_1 should be sufficiently larger than T_3, and T_2 value should be placed between T_1 and T_3. Moreover, the response speed of EDLC power control loop determines how much disturbance the ESS absorbs. If the response speed is too fast, the power of energy storage will not be appeared because the EDLC power is zero in steady state. Based on these assumptions, the time constants are determined as $T_1 = 20$ s, $T_2 = 4$s, and $T_3 = 0.01$s in order to satisfy $T_1 > T_2 > T_3$. The corresponding values of gains are obtained as $K_1 = 1/T_1 = 0.05$ and $K_3 = 1/T_3 = 100$. The proportional gain of EDLC power controller is set as $K_p = 0.01$.

From the above mentioned feedback control scheme, the overall control diagram can be represented as shown in Fig. 12. In Fig. 12, the output of dc link energy control loop is the current signal. Therefore, the gain K_4 is used to convert from the dimension of current signal (ampere) to the duty command d^*.

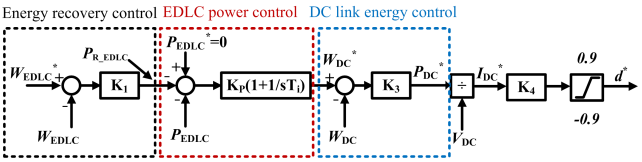

FIGURE 12. Overall control block diagram of ESS.

D. STABILITY ANALYSIS OF ESS CONTROL LOOP

The feedback control structure of ESS was presented in Fig. 8. In Fig. 8, the EDLC power controller and the dc link energy control are the main control loops for the control of ESS. The EDLC energy recovery control loop is an additional control loop for recovering the energy to its steady state after transient period. Therefore, only the main control loops are considered in the stability and performance analysis of closed-loop system and the transfer function of $P_{EDLC}{}^*$ to W_{DC} is obtained as follows:

$$\frac{W_{DC}}{P^*_{EDLC}} = \frac{\left(K_3K_pT_2\right)\, s + K_3K_p}{\left(K_3K_pT_2\right)\, s^2 + \left(K_3T_2 + K_3K_p\right) s} \tag{17}$$

Using (17), the root locus diagrams of the closed-loop transfer function for each control parameter is described in Fig. 13. The characteristic equation includes two roots on the real axis. One is located at the origin, which is fixed, and does not influence by changing the three parameters. However, the second root is highly dependent to the parameters selection. As shown in Fig. 13, the poles are remained on the left-half plane for a wide range of each parameter variation. However, the performance and stability margin may be affected by selecting different values. As shown in Fig. 13, the parameters T_2, K_p and K_3 have been selected such that the stability and performance of the control system to be not degraded.

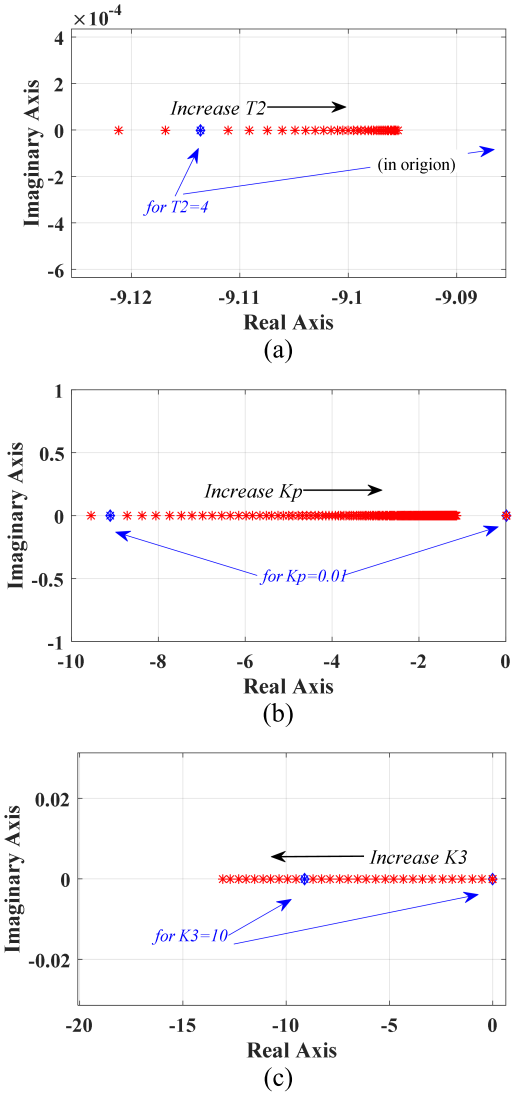

FIGURE 13. The root locus diagrams of the ESS closed-loop system (a) T_2 varies from 0.01 to 10, (b) K_p varies from 0.05 to 1, (c) K_3 varies from 1 to 1200.

E. GENERATION OF SWITCHING SIGNALS FOR BIDIRECTIONAL CHOPPER

The switching signals for the bidirectional chopper are generated as shown in Fig. 14. In Fig. 14, S_1 and S_2 are the upper and lower switching signals of the chopper, $V_{DC}{}^*$ is the reference dc link voltage, V_{DC} is the actual dc link voltage, d^* is the duty cycle. The reference dc link voltage $V_{DC}{}^*$ is calculated from the reference dc link energy $W_{DC}{}^*$. As illustrated in the figure, the sign of the duty cycle d^* indicates the operation mode of bidirectional chopper; negative sign

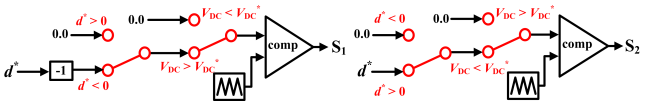

FIGURE 14. Scheme of switching signals generation.

for the buck mode and positive sign for the boost mode. In the buck mode, V_{DC} is greater than V_{DC}^* and the EDLC charges power from the dc link. In the boost mode, V_{DC} is less than V_{DC}^* and the EDLC discharges power to the dc link.

V. CALCULATION OF ENERGY STORAGE CAPACITY

In order to calculate the required capacity of energy storage, the load change is assumed to be in a step shape as shown in Fig. 15. In Fig. 15, P_{LOAD} is load power, P_{gen} is engine generator output power and τ_g is a generator time constant. As can be seen in the figure, P_{gen} responds to the step change of P_{LOAD} with delay.

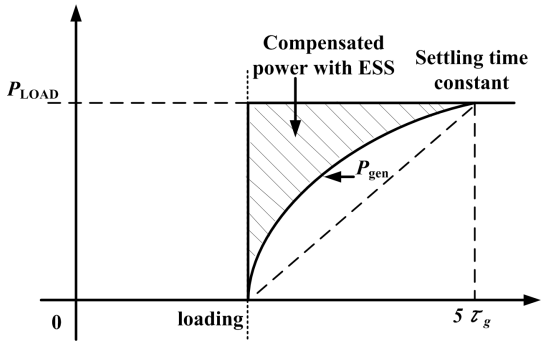

FIGURE 15. Step load power response of generator.

The incremental difference between the load power and generator output power is considered as the kinetic energy of rotor which causes variations in rotational speed of engine generator. The rotational speed variations of engine generator can be suppressed if the kinetic energy of rotor is compensated by using the ESS. Based on this assumption, the capacity of energy storage can be calculated as described in the following subsections.

A. CALCULATING KINETIC ENERGY OF ROTOR

As shown in Fig. 15, the kinetic energy of rotor for step load change can be calculated by using τ_g because the rotational speed response depends on τ_g. The speed approximately returns to its steady state after five times of τ_g under the assumption that the change is approximated as an exponential curve. Thus, it can be considered that the kinetic energy of rotor is generated during the period of $5\tau_g$. For simplicity, the kinetic energy is calculated by assuming in a triangular area as shown in Fig. 15. If the values of τ_g and the rated load power P_{LOAD} are known, the kinetic energy of rotor can be calculated as given in (17). In this study, the value of τ_g is set as 1 s and P_{LOAD} is 10 kW, and therefore the required energy W is calculated as

$$W = \frac{1}{2} \times P_{LOAD} \times 5\tau_g = 25000\,[\mathrm{J}] \tag{18}$$

The obtained kinetic energy is considered as the required amount of energy to be compensated by the ESS.

B. CALCULATING MAXIMUM VOLTAGE LIMIT OF EDLCs SYSTEM

When Space Vector PWM is adopted, the maximum dc link voltage V_{DC} can be determined according to the generator rated voltage V_{AC-RMS} as

$$V_{DC} = \sqrt{2}\, V_{AC-RMS} \tag{19}$$

In this work, the value of V_{AC-RMS} is fixed at 210 V. Thus, the calculated V_{DC} is 297 V. The maximum EDLC voltage limit V_{max} should be less than V_{DC} because the boost chopper is connected between the EDLC and dc link. Therefore, V_{max} is chosen as 200 V, and the minimum EDLC voltage limit V_{min} is chosen as 100 V (50 percent of V_{max}). Then, in order to calculate the stand-by energy, the stand-by voltage V_0 can be calculated by using the capacitor energy equation. Separating charging and discharging cases, only half of total energy is used to calculate V_0 as

$$\frac{1}{2}CV_0^2 = \left(\frac{1}{2}CV_{max}^2 + \frac{1}{2}CV_{min}^2\right) \times \frac{1}{2} \tag{20}$$

$$V_0 = \sqrt{\frac{V_{min}^2 + V_{max}^2}{2}} \tag{21}$$

Substituting the values of V_{max} and V_{min}, the value of V_0 is obtained as 160 V.

Using V_0 and V_{min}, the total capacitance of EDLC C_{tot} can be calculated as

$$C_{tot} = \frac{2W}{(V_0^2 - V_{min}^2)} \tag{22}$$

By the above equation, C_{tot} of EDLC is calculated as 3.5 F.

C. CALCULATING MINIMUM NUMBER OF EDLC UNITS

The value of V_{max} is used for determining the numbers of EDLC for series connection. For practical applications, the rating of EDLC voltage should be greater than the maximum EDLC voltage limit V_{max}. In this study, the rating of EDLC voltage is set as 1.25 times of V_{max}. Then, the numbers of EDLC for series connection n_s can be expressed as

$$n_s = \frac{1.25 \times V_{max}}{v_1} \tag{23}$$

Here, v_1 is the rated voltage of one EDLC. In this study, V_{max} is 200 V and v_1 is 2.5 V, then $n_s = 100$. When 100 numbers of EDLC units with 350 F for each EDLC are connected in series, the total capacitance is 3.5 F which is matched with C_{tot}, the calculated total capacitance of EDLC.

VI. SIMULATION RESULTS

The circuit diagram illustrated in Fig. 1 is used in simulation. In order to verify the performance of the proposed control scheme, some simulations are carried out for two cases of with EDLC and without EDLC. The transient responses of the closed-loop system are investigated under both load connection and load removal conditions. For both cases, at 90 s, the load is connected to or disconnected from the system.

For the 10 kW base power of the system, the step responses are analyzed by using a 9-kW (0.9 pu) resistive load. The parameters of PMSG and VSG control were listed in Tables 2 and 3 in section III. The parameters of ESS control are listed in Table 4.

TABLE 4. Parameters of energy storage used in simulation.

Minimum EDLC voltage, V_{min}	100 V	Maximum EDLC voltage, V_{max}	200 V
Stand-by voltage of EDLC, V_0	160 V	Gain, k_4	100
Gain of $W_{DC}{}^*$ control k_3	1000	Total capacitance of EDLC	3.5 F
Gain of P_{EDLC} control, k_p	0.01	Time constant of P_{EDLC} control, T_2	2 s
Gain of recovery control, W_{EDLC} ,k_1	0.08	Chopper switching frequency, f	15 kHz
Reactor inductance, L	0.39 mH		

First, the results of loading case are presented. In Fig. 16, the engine speed response to load connection is depicted. In Fig. 16(a), the engine speed decreases from its rated value of 1710 min^{-1} to 1450 min^{-1}. In Fig. 16(b), the engine speed decreases from 1710 min^{-1} to 1610 min^{-1}. Therefore, the speed dip due to loading is reduced by 160 min^{-1} using EDLC.

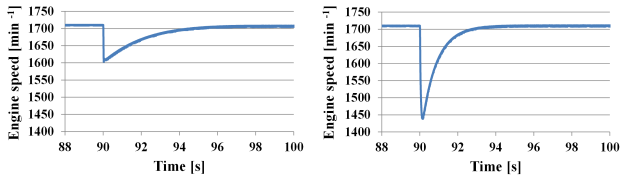

FIGURE 16. Engine speed response to load connection.

The dc link voltage response is shown in Fig. 17. Before connecting the load, the value of dc link voltage is 390 V for both cases. The dc link voltage drops to 300 V at the start of loading in the case of without EDLC. After that, it returns back to around 320 V. With EDLC, the dc voltage firstly drops to about 340 V, and then it gradually decreases to around 320 V. The waveforms in Fig. 17 show that the dc link voltage has a smooth change in the case of using EDLC.

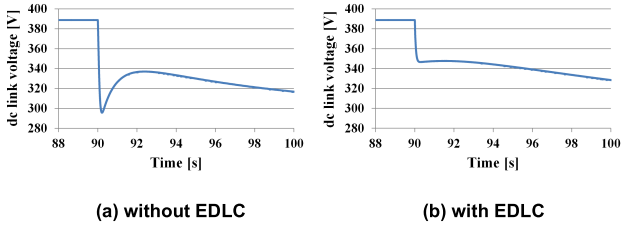

FIGURE 17. DC link voltage response to load connection.

The engine speed and dc voltage for load removal case are illustrated in Figs. 18 and 19, respectively. Fig. 18(a) shows

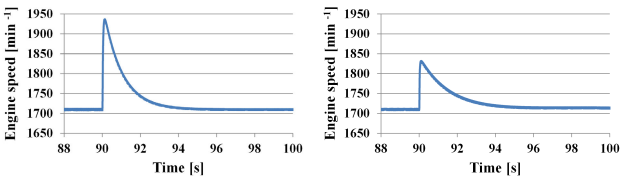

FIGURE 18. Engine speed response to load removal condition.

that the engine speed increases from 1710 min^{-1} to 1940 min^{-1} when the load is removed from the system. In Fig. 18(b), the engine speed increases from 1710 min^{-1} to 1830 min^{-1}. These results show that the speed rise is reduced by 110 min^{-1} using EDLC.

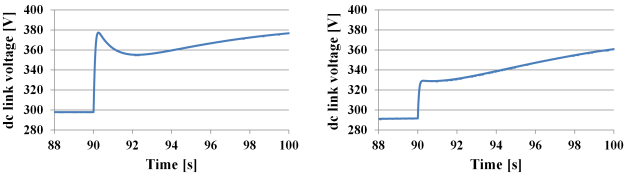

FIGURE 19. DC link voltage response to load removal condition.

In Fig. 19(a), there is a small overshoot in dc voltage when the load is removed from the system. In Fig. 19(b), the dc voltage has no overshoot and returns back to its steady state value after removing the load from the system.

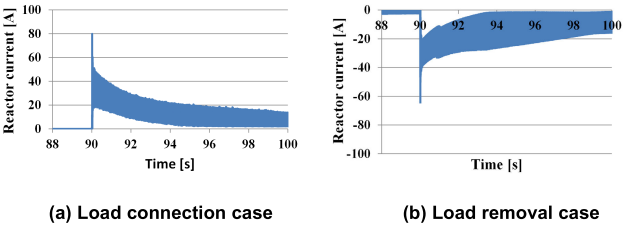

FIGURE 20. EDLC current response to load transient.

In Fig. 20, the reactor current of EDLC is shown. In the load connection case, the positive current indicates that the EDLC energy is transferred to the dc link. At the instant of loading, the current rises to 80 A, and decreases to get back zero state after transient. For the load removal case, the negative current indicates that the EDLC absorbs power from the dc link. The current decreases to −60 A when the load is removed from the system. After transient period, it is returned to reach the zero state. From the waveforms of EDLC voltage and current, it is confirmed that the bidirectional chopper works well in the boost mode for the loading case, and in the buck mode for the load removal case.

Fig. 21 shows the EDLC voltage waveforms of both the loading and load removal cases. The EDLC voltage decreases from its stand-by voltage of 160 V to 120 V in the load

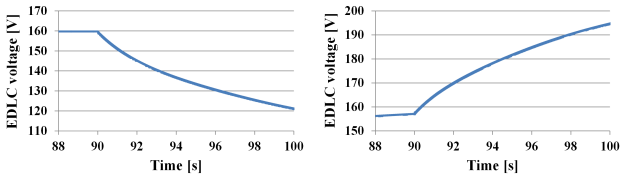

(a) Load connection case (b) Load removal case

FIGURE 21. EDLC voltage response to load transient.

connection case, and the voltage increases from its stand-by voltage to nearly 195 V in the case of load removal.

By using the EDLC voltage variations, the delivered energy and the absorbed energy of ESS can be calculated. The delivered energy for the load connection case can be calculated as

$$W = \frac{1}{2}C \times \left(160^2 - 120^2\right) = 19600\,[\mathrm{J}]$$

The absorbed energy for the load removal case can be calculated as

$$W = \frac{1}{2}C \times \left(195^2 - 158^2\right) = 22857\,[\mathrm{J}]$$

From these calculation results, the amount of energy for both load connection and load removal cases are within the amount of estimated energy in section V.

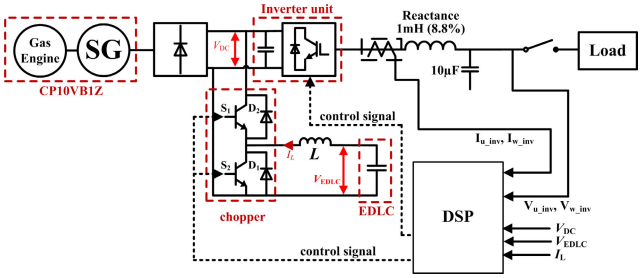

FIGURE 22. Experimental circuit configuration with real engine set.

VII. EXPERIMENTS

An experimental study was conducted in order to verify the effectiveness of the proposed control system. The experimental circuit diagram is shown in Fig. 22. The real engine generator set of model number CP10VB1Z manufactured by Yanmar Company was used in the experiment. The system operation conditions for the experiment were the same as those explained in the simulation study. The parameters of PMSG, VSG controller and ESS control were also the same as assumed in the simulation study. As presented in section V, the ESS used in experimental study is composed of 100 units of EDLCs connected in series. The rated voltage of each EDLC is 2.5 V. The total capacitance of energy storage is 3.5 F. The configuration of EDLC used in experiment is shown in Fig. 23.

The variations of engine speed for the load connection case are shown in Fig. 24. In Fig. 24(a), without EDLC,

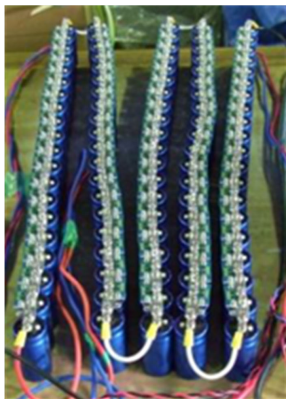

FIGURE 23. Configuration of EDLC.

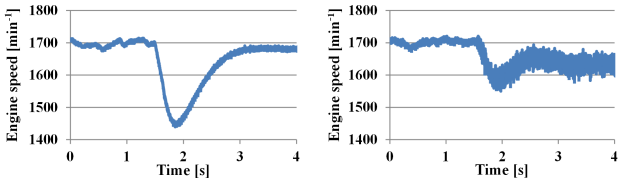

(a) without EDLC (b) with EDLC

FIGURE 24. Engine speed response to load connection (experiment).

the engine speed decreased from its rated value of 1710 min^{-1} to 1450 min^{-1}. In Fig. 24(b), with EDLC, the engine speed decreased from 1710 min^{-1} to 1550 min^{-1}. Therefore, the engine speed deviation was reduced 100 $\mathrm{min}^{-1}$by using the EDLC. In Fig. 25, before connecting the load, the value of dc voltage was kept at 390 V for both the cases. When the load was connected to the system without the EDLC, the dc voltage suddenly decreased to 260 V and then returned to nearly 300 V, whereas in the case with the EDLC, the dc voltage gradually decreased to 300 V.

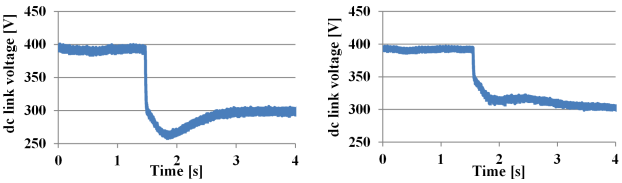

(a) without EDLC (b) with EDLC

FIGURE 25. DC voltage response to load connection (experiment).

The results of load removal case are shown in Figs. 26 and 27, respectively. In Fig. 26(a), at the time of load disconnection, the engine speed rose to 2000 min^{-1} at first, and then it decreased continuously because the engine operation stopped. It shows that the engine speed variation exceeded its maximum allowable limit. However, under the operation with EDLC, the speed rose to 1800 min^{-1} and the system maintained in operation as shown in Fig. 26(b). In Fig. 27(a), the dc link voltage rose to nearly 470 V when the load was removed from the system because the operation broke down. In Fig. 27(b), the dc link voltage returned to its

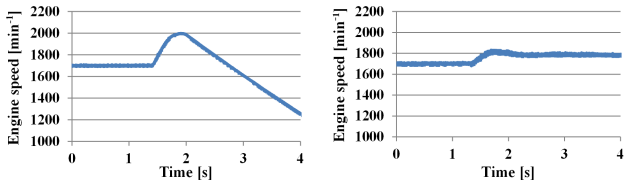

FIGURE 26. Engine speed response to load removal (experiment).

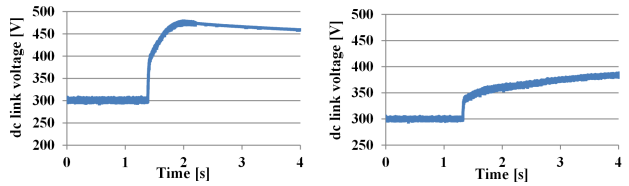

FIGURE 27. DC link voltage response to load removal (experiment).

steady state value of 390 V after removing the load from the system.

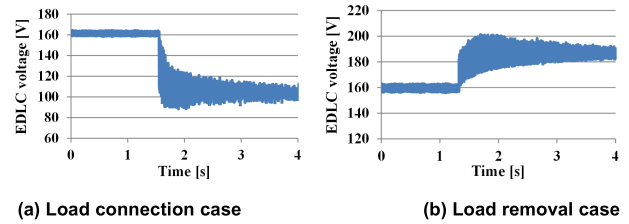

FIGURE 28. EDLC voltage response to load transient (experiment).

The results of measured EDLC voltages are shown in Fig. 28. For load connection case, the EDLC voltage dropped from its stand-by voltage of 160 V to nearly 100 V (minimum limit) as the energy storage is providing power to the dc link. In the case of load removal, the EDLC voltage is increased from 160 V to nearly 195 V, which means the EDLC was charged from the dc link.

In the same way as simulation study, the delivered energy for the loading case can be calculated as

$$W = \frac{1}{2}C \times \left(160^2 - 102^2\right) = 26593\,[\mathrm{J}]$$

The absorbed energy for the load removal case can be calculated as

$$W = \frac{1}{2}C \times \left(188^2 - 160^2\right) = 17052\,[\mathrm{J}]$$

From experimental results, the amount of energy for load connection case is almost close to the amount of estimated energy. The amount of energy for load removal case is within the amount of estimated energy in section V.

Since the main aim of this study is to reduce gas-engine speed variations under sudden load changes, the results of speed deviations under load transients are summarized in Table 5. The results of loading cases prove that the proposed control scheme can significantly reduce gas-engine speed deviations by adding an external ESS to the dc link that connected with VSG control.

TABLE 5. Speed variation in ratio for 9 kW load.

Loading	Simulation	Experiment
Without EDLC	Decrease 260 min^{-1} (15.2% of rated speed)	Decrease 260 min^{-1} (15.2% of rated speed)
With EDLC	Decrease 90 min^{-1} (5.3% of rated speed)	Decrease 160 min^{-1} (9.4% of rated speed)

VIII. CONCLUSION

In order to improve the transient performance of a stand-alone gas engine generator at the instant of sudden load change, the VSG control method in combination with an external ESS is proposed in this paper. The dynamic characteristics of the proposed gas engine generator system were investigated under load connection and load removal cases for the 0.9 pu load step change. The investigations were done by both simulation and experimental studies. The obtained simulation and experimental results verified that the proposed control structure compensated the slow response of engine's mechanical system by providing a temporary energy during transient state. As a result, the engine speed variations were well suppressed and the system was operating without shutting down for the 0.9 pu load step change. Therefore, the proposed control scheme can improve the transient characteristics of a stand-alone gas engine generator system.

REFERENCES

[1] *Transient Response Behaviour of Gas Engines, Position Paper*, CIMAC, Frankfurt, Germany, Apr. 2011.
[2] A. Leitner-Audoui, M. Perktold, J. Huber, and J. Thalhauser, "Highly transient load response," in *Proc. 29th CIMAC World Congr.*, Vancouver, BC, Canada, Jun. 2019, pp. 1–10.
[3] A. Mondal, A. A. Renjit, M. S. Illindala, and J. H. Eto, "Operation and impact of energy storage system in an industrial microgrid," in *Proc. IEEE Ind. Appl. Soc. Annu. Meeting*, Addison, TX, USA, Oct. 2015, pp. 18–22.
[4] J. Leuchter, P. Bauer, V. Rerucha, and V. Hajek, "Dynamic behavior modeling and verification of advanced electrical-generator set concept," *IEEE Trans. Ind. Electron.*, vol. 56, no. 1, pp. 266–279, Jan. 2009.
[5] J. Lee, S. Lee, and S. Sul, "Variable-speed engine generator with supercapacitor: Isolated power generation system and fuel efficiency," *IEEE Trans. Ind. Appl.*, vol. 45, no. 6, pp. 2130–2135, Nov./Dec. 2009.
[6] G. Delille, B. Francois, and G. Malarange, "Dynamic frequency control support by energy storage to reduce the impact of wind and solar generation on isolated power system's inertia," *IEEE Trans. Sustain. Energy*, vol. 3, no. 4, pp. 931–939, Oct. 2012.
[7] J. Driesen and K. Visscher, "Virtual synchronous generators," in *Proc. IEEE Power Energy Soc. Gen. Meeting, Convers. Del. Energy*, Pittsburgh, PA, USA, Jul. 2008, pp. 1–3.
[8] H.-P. Beck and R. Hesse, "Virtual synchronous machine," in *Proc. 9th Int. Conf. Elect. Power Qual. Util.*, Barcelona, Spain, 2007, pp. 1–6.
[9] Q.-C. Zhong and G. Weiss, "Synchronverters: Inverters that mimic synchronous generators," *IEEE Trans. Ind. Electron.*, vol. 58, no. 4, pp. 1259–1267, Apr. 2011.
[10] K. Sakimoto, Y. Miura, and T. Ise, "Stabilization of a power system including inverter type distributed generators by the virtual synchronous generator," (in Japanese), *IEEE J. Trans. Power Energy*, vol. 132, no. 4, pp. 341–349, Apr. 2012.
[11] T. Shintai, Y. Miura, and T. Ise, "Oscillation damping of a distributed generator using a virtual synchronous generator," *IEEE Trans. Power Del.*, vol. 29, no. 2, pp. 668–676, Apr. 2014.

[12] J. Liu, Y. Miura, and T. Ise, "Comparison of dynamic characteristics between virtual synchronous generator and droop control in inverter-based distributed generators," *IEEE Trans. Power Electron.*, vol. 31, no. 5, pp. 3600–3611, May 2016.
[13] J. Liu, Y. Miura, H. Bevrani, and T. Ise, "Enhanced virtual synchronous generator control for parallel inverters in microgrids," *IEEE Trans. Smart Grid*, vol. 8, no. 5, pp. 2268–2277, Sep. 2017.
[14] Y. Hirase, K. Sugimoto, K. Sakimoto, and T. Ise, "Analysis of resonance in microgrids and effects of system frequency stabilization using a virtual synchronous generator," *IEEE J. Emerg. Sel. Topics Power Electron.*, vol. 4, no. 4, pp. 1287–1298, Dec. 2016.
[15] N. Soni, S. Doolla, and C. M. Chandorkar, "Improvement of transient resonse in microgrids using virtual inertia," *IEEE Trans. Power Del.*, vol. 28, no. 3, pp. 1830–1838, Jul. 2013.
[16] J. Liu, Y. Miura, and T. Ise, "Fixed-parameter damping methods of virtual synchronous generator control using state feedback," *IEEE Access*, vol. 7, pp. 99177–99190, 2019.
[17] D. Chen, Y. Xu, and A. Q. Huang, "Integration of DC microgrids as virtual synchronous machines into the AC grid," *IEEE Trans. Ind. Electron.*, vol. 64, no. 9, pp. 7455–7466, Sep. 2017.
[18] J. A. Suul, S. D'Arco, and G. Guidi, "Virtual synchronous machine-based control of a single-phase bi-directional battery charger for providing vehicle-to-grid services," *IEEE Trans. Ind. Appl.*, vol. 52, no. 4, pp. 3234–3244, Jul./Aug. 2016.
[19] M. Guan, W. Pan, J. Zhang, Q. Hao, J. Cheng, and X. Zheng, "Synchronous generator emulation control strategy for voltage source converter (VSC) stations," *IEEE Trans. Power Syst.*, vol. 30, no. 6, pp. 3093–3101, Nov. 2015.
[20] M. A. Torres L, L. A. C. Lopes, L. A. Morán T, and J. R. Espinoza C, "Self-tuning virtual synchronous machine: A control strategy for energy storage systems to support dynamic frequency control," *IEEE Trans. Energy Conv.*, vol. 29, no. 4, pp. 833–840, Dec. 2014.
[21] R. Shi, X. Zhang, L. Fang, H. Xu, C. Hu, Y. Tu, and H. Ni, "Research on power compensation strategy for diesel generator system based on virtual synchronous generator," in *Proc. IEEE 8th Int. Power Electron. Motion Control Conf. (IPEMC-ECCE Asia)*, Hefei, China, May 2016, pp. 939–943.
[22] D. Li, Q. Zhu, S. Lin, and X. Y. Bian, "A self-adaptive inertia and damping combination control of VSG to support frequency stability," *IEEE Trans. Energy Convers.*, vol. 32, no. 1, pp. 397–398, Mar. 2017.
[23] J. Fang, Y. Tang, H. Li, and X. Li, "A bttery/ultracapacitor hybrid energy storage system for implementing the power management of virtual synchronous generators," *IEEE Trans. Power Electron.*, vol. 33, no. 4, pp. 2820–2824, Apr. 2018.
[24] Y. Ma, W. Cao, L. F. Yang, F. Wang, and L. M. Tolbert, "Virtual synchronous generator control of full converter wind turbines with short-term energy storage," *IEEE Trans. Ind. Electron.*, vol. 64, no. 11, pp. 8821–8831, Nov. 2017.
[25] Y. Guo, L. Chen, K. Li, T. Zheng, and S. Mei, "A novel control strategy for stand-alone photovoltaic system based on virtual synchronous generator," in *Proc. IEEE Power Energy Soc. Gen. Meeting (PESGM)*, Boston, MA, USA, Jul. 2016, pp. 17–21.
[26] H. S. Hlaing, Y. Miura, and T. Ise, "A permanent magnet synchronous generator control approach for stand-alone gas engine generation system," in *Proc. IEEE 8th Int. Power Electron. Motion Control Conf. (IPEMC-ECCE Asia)*, Hefei, China, vol. 25, May 2016, pp. 3427–3434.
[27] H. Bevrani, B. Francois, and T. Ise, *Microgrid Dynamics and Control*. Hoboken, NJ, USA: Wiley, 2017.

HTAR SU HLAING received the B.E. and M.E degrees in electrical power engineering from Mandalay Technological University, Myanmar, in 2004 and 2009, respectively. She is currently pursuing the Ph.D. degree with Osaka University, Japan.

Her research interests include power electronics, control systems for engine generators, and virtual synchronous generators for distributed generation systems.

JIA LIU (S'15–M'17) received the B.Eng. and M.Eng. degrees from Xi'an Jiaotong University, Xi'an, China, in 2008 and 2011, respectively, the Diplôme d'Ingénieur degree from the University of Technology of Troyes, Troyes, France, in 2011, and the Ph.D. degree in engineering from Osaka University, Osaka, Japan, in 2016.

He was with Delta Electronics (Jiangsu), Ltd., Nanjing, China, from 2011 to 2012. Since 2016, he has been with the Division of Electrical, Electronic, and Information Engineering, Graduate School of Engineering, Osaka University, where he is currently an Assistant Professor. His research interests include distributed generators, microgrids, power quality, and motor drives.

YUSHI MIURA received the bachelor's, master's, and Ph.D. degrees from the Tokyo Institute of Technology, in 1990, 1992, and 1995, respectively.

He was a Researcher with the Japan Atomic Energy Research Institute, from 1995 to 2004, and an Associate Professor with Osaka University, from 2004 to 2018. He is currently a Professor with the Nagaoka University of Technology. His research interests include power electronics, power engineering, energy storage systems, microgrids, smart grids, and superconducting coil power supplies.

HASSAN BEVRANI (S'90–M'04–SM'08) received the Ph.D. degree in electrical engineering from Osaka University, Japan, in 2004.

He is currently a Full Professor and the Program Leader of the Smart/Micro Grids Research Center (SMGRC), University of Kurdistan (UOK). He was a Senior Research Fellow and a Visiting Professor with Osaka University, Kumamoto University, Japan, the Queensland University of Technology, Australia, the Kyushu Institute of Technology, Japan, Centrale Lille, France, and the Technical University of Berlin, Germany. He is the author of six international books, 15 book chapters, and more than 300 journal/conference papers. His current research interests include smart grid operation and control, power systems stability and optimization, microgrid dynamics and control, and intelligent/robust control applications in power electric industry.

TOSHIFUMI ISE (M'86) received the B.E., M.E., and Ph.D. degrees in electrical engineering from Osaka University, Osaka, Japan, in 1980, 1982, and 1986, respectively.

He is an Emeritus Professor with Osaka University and the President of NARA-GAKUEN Incorporated Educational Institution. From 1986 to 1990, he was with the Nara National College of Technology, Nara, Japan. Since 1990, he has been with the Faculty of Engineering, Graduate School of Engineering, Osaka University, where he was a Professor, from August 2002 to March 2018. His research interest includes power electronics and applied superconductivity for power systems.

Dr. Ise is a Fellow of the Institute of Electrical Engineers of Japan (IEEJ).